

# Microscopic analysis of quadrupole collective motion in Cr-Fe nuclei

## II. Doorway nature of mixed-symmetry states

Hitoshi Nakada

*Department of Physics, Faculty of Science, Chiba University*

*Yayoi-cho 1-33, Inage-ku, Chiba 263, Japan*

Takaharu Otsuka

*Department of Physics, Faculty of Science, University of Tokyo*

*Hongo 7-3-1, Bunkyo-ku, Tokyo 113, Japan*

(November 17, 2018)

### Abstract

The mixed-symmetry collective modes are investigated in Cr-Fe nuclei, by analyzing the realistic shell-model wavefunctions via the  $H^n$ -cooling method. It is clarified that the relatively low-lying mixed-symmetry states behave like doorway states. For these nearly spherical nuclei, the lowest mixed-symmetry state is shown to have  $J^P = 2^+$ . An indication of the mixed-symmetry  $3^+$  state is obtained. The sequence of the mixed-symmetry  $2^+$ ,  $1^+$  and  $3^+$  levels and its nucleus-dependence are discussed. Calculated  $M1$  and  $M3$  transitions in the low-energy region suggest that the mixed-symmetry  $1^+$  and  $3^+$  components are detectable. We investigate the  $B(M1)$  distribution in a wider energy range, without breaking the isospin quantum number. It is confirmed that the mixed-symmetry  $1^+$  component is well separated from the peak of the spin excitation. The isospin-raising component has a peak, separated well from the isospin-conserving one. The orbital angular-momentum contributes

destructively to the spin excitations.

PACS numbers: 21.10.Re, 21.60.Cs, 21.60.Ev, 27.40.+z

## I. INTRODUCTION

While the mixed-symmetry (MS) states of the proton-neutron interacting boson model (IBM-2) have been studied for more than a decade, there still remain various aspects to be explored on this type of collective mode. The  $1^+$  states discovered around  $E_x \simeq 3$  MeV in rotational nuclei [1] correspond to a MS state (scissors mode), which has been predicted by the IBM-2 [2] as well as by other models [3]. Significant fragmentation of the  $B(M1)$  strength, however, has been observed. The MS  $2^+$  state has remained much less investigated so far, though this  $2^+$  state may be lower than any other MS states in spherical nuclei [4]. In terms of the geometrical picture, the MS  $2^+$  state in a spherical nucleus is interpreted as the quadrupole oscillation out of phase between protons and neutrons [5]. Experimental studies in the Cr-Fe region have suggested the presence and rather weak fragmentation of the MS  $2^+$  state [6]. We have reported a realistic shell-model result on this state in  $^{56}\text{Fe}$  [7].

We shall study, in this paper, the MS states of Cr-Fe nuclei in more detail. These nuclei provide us with a precious clue to understanding some basic features of the nuclear quadrupole collective motion from microscopic standpoints. On one side, salient quadrupole collectivity can be formed in these nuclei. On the other side, these nuclei are accessible by a realistic shell-model calculation [8], which becomes prohibitively difficult in heavier nuclei. In order to discuss quadrupole collective modes based on the shell model, the  $H^n$ -cooling method ( $H^n\text{CM}$ ), which has been proposed in the previous paper [9], will be used. The wavefunctions of the MS states have been generated explicitly with the renormalization based on the  $H^n\text{CM}$ . It is straightforward to compare these wavefunctions with those of the realistic shell model. We thus investigate some properties of the relatively low-lying MS states in connection to the realistic shell-model calculation.

## II. SHELL-MODEL CALCULATION AND RENORMALIZATION

It has been shown that a large-scale shell-model calculation with a realistic interaction derived from the  $G$ -matrix [10] is successful in the middle  $pf$ -shell region [7,8]. The  $k \leq 2$  model space has been assumed, where  $k$  denotes the number of nucleons excited from  $0f_{7/2}$  to the upper  $pf$ -shell orbits. For even-even nuclei, the energy levels with  $E_x < 4$  MeV are described to a good accuracy, with typical deviation of 0.3 MeV [8]. The large configuration space is crucial to reproduce the levels in the energy region of  $3 < E_x < 4$  MeV, where the MS states likely appear. The energy levels of  $^{58}\text{Fe}$  and  $^{56}\text{Cr}$  are also shown in Ref. [9].

We shall investigate the MS quadrupole collective modes, based on this realistic shell-model result. In the OAI mapping [11], a correspondence is postulated between the IBM-2 states and the fermion states comprised of the  $SD$ -pairs. The realistic shell-model hamiltonian, however, contains various correlations, which are not carried by the naive  $S$ - and  $D$ -pairs. The total probability of the  $SD$ -components is substantially smaller than unity even in the shell-model  $0_1^+$  and  $2_1^+$  states. In order to incorporate effects of the non- $SD$  components, we renormalize the wavefunctions of the  $SD$ -states. The leakage out of the  $SD$  space occurs because of the excitation from  $0f_{7/2}$ , as well as of the admixture of like-nucleon pairs other than  $S$  and  $D$ . The excitation out of the  $^{56}\text{Ni}$  core amounts to about 40% in the ground states [8], whereas the influence of other nucleon pairs without the core excitation is small in the  $0_1^+$  and  $2_1^+$  states. This relatively large core-excitation probability requires a method beyond the perturbation theory. The  $\text{H}^n\text{CM}$  developed in the previous paper [9] enables us to renormalize wavefunctions of the quadrupole collective states and to discuss the MS states to the same extent as the  $0_1^+$  and  $2_1^+$  states.

We shall briefly discuss here the renormalization associated with the  $\text{H}^n\text{CM}$  briefly, which has been introduced in Ref. [9]. In the description assuming the  $^{56}\text{Ni}$  inert core, the  $^{56}\text{Fe}$  nucleus has a pair of proton holes and a pair of neutron valence particles. The  $S$ - and  $D$ -pairs of protons are defined as the  $0^+$  and  $2^+$  states of the  $(0f_{7/2})^{-2}$  configuration, while those of neutrons are collective  $0^+$  and  $2^+$  states of the  $(0f_{5/2}1p_{3/2}1p_{1/2})^2$  configuration. The  $SD$

space is then constructed by these proton and neutron  $S$ - and  $D$ -pairs. The proton-neutron symmetry is taken into consideration for the  $SD$ -states through the  $F$ -spin values of their IBM-2 images [9]. The states having  $F = F_{\max}$  are called totally-symmetric states in the IBM-2, while those with  $F = F_{\max} - 1$  are MS states. Here  $F_{\max} = \frac{1}{2}N^B = \frac{1}{2}(N_{\pi}^B + N_{\nu}^B)$ , with  $N^B$  denoting boson (*i.e.*, like-nucleon pair) number. The lowest-lying quadrupole collective states have been known to be predominantly totally-symmetric states. We will mainly deal with some lower-lying states characterized by  $F = F_{\max} - 1$ . One might notice that, because  $F_{\max} = 1$ , the  $F = F_{\max} - 1$  states of  $^{56}\text{Fe}$  turn out to be totally anti-symmetric. However, they are classified as mixed-symmetry states in this article, because they belong to the class of the  $F = F_{\max} - 1$  states.

In the  $H^n\text{CM}$ , the primary bases [9] (denoted by  $\Psi_{\lambda}^{(0)}$  with  $\lambda = 1, 2, \dots, l$ ) are assumed at the beginning. The bases consisting of the  $SD$ -pairs will be taken as primary bases in the present case. If  $e^{-\beta H}$  acts on a primary basis, each basis yields a superposition of a number of exponentially-decaying components. In the  $H^n\text{CM}$  with a given  $n$ , we consider  $n$  non-primary bases (denoted by  $\phi_{\lambda}^{(1)}, \phi_{\lambda}^{(2)}, \dots, \phi_{\lambda}^{(n)}$ ) for each  $\Psi_{\lambda}^{(0)}$ , through the power-series expansion of  $e^{-\Delta\beta H}$  up to  $O((\Delta\beta)^n)$ . The  $\phi_{\lambda}^{(\nu)}$  basis is generated from  $H^{\nu}|\Psi_{\lambda}^{(0)}\rangle$ . In this procedure, an appropriate orthonormalization is applied. We thus have the following primary and non-primary orthonormal bases,

$$\begin{aligned}
&\Psi_1^{(0)}, \Psi_2^{(0)}, \dots, \Psi_l^{(0)}, \\
&\phi_1^{(1)}, \phi_2^{(1)}, \dots, \phi_l^{(1)}, \\
&\phi_1^{(2)}, \phi_2^{(2)}, \dots, \phi_l^{(2)}, \\
&\dots\dots\dots, \\
&\phi_1^{(n)}, \phi_2^{(n)}, \dots, \phi_l^{(n)}.
\end{aligned} \tag{1}$$

For each  $\lambda$ , we solve the eigenvalue problem within the space  $\Gamma_{\lambda}^{(n)} \equiv \{\Psi_{\lambda}^{(0)}, \phi_{\lambda}^{(1)}, \phi_{\lambda}^{(2)}, \dots, \phi_{\lambda}^{(n)}\}$ , having  $(n+1)$  eigenvectors. The lowest one is adopted as the renormalized basis  $\Psi_{\lambda}^{(n)}$ . Once the renormalized bases are obtained, the renormalized space is comprised of  $\Psi_{\lambda}^{(n)}$ 's. This space closes up to  $O((\Delta\beta)^n)$ , for the operation of  $e^{-\Delta\beta H}$ .

In the application of the  $H^n$ CM to the  $SD$ -space of the Cr-Fe nuclei [9], the angular-momentum conservation is treated exactly in the whole procedure of the  $H^n$ CM, by choosing the bases with good angular momentum for  $\Psi_\lambda^{(0)}$ 's. Note that, because the proton and neutron pairs are formed by different orbits, all the  $SD$ -states have the same isospin for a given nucleus. This situation is also maintained during the  $H^n$ CM. Moreover, the proton-neutron symmetry (*i.e.*,  $F$ -spin), which concerns our main interest of this paper, is also taken into consideration in choosing the primary bases.

The effective hamiltonian within the renormalized  $SD$  space is given by the matrix elements  $\langle \Psi_{\lambda'}^{(n)} | H | \Psi_\lambda^{(n)} \rangle$ . The energy levels and corresponding wavefunctions in the renormalized  $SD$  space are calculated by diagonalizing the matrix thus obtained. Therefore each of these eigenfunctions is a linear combination of  $\Psi_\lambda^{(n)}$ 's. In the following sections, we shall inspect the eigenfunctions within the renormalized  $SD$  space, focusing on the MS components. The actual  $H^n$ CM procedure is carried out for  $n = 2$  (*i.e.*,  $H^2$ CM) in this study.

As shown in Ref. [9], the  $H^2$ CM provides us with remarkable improvement on the  $0_1^+$  and  $2_1^+$  wavefunctions from the unrenormalized ones, in comparison with more complete shell-model results (see Table I of Ref. [9]). The energy levels are also in good agreement, between the  $H^2$ CM and the shell-model results (see Figs. 1, 2, 5 and 6 of Ref. [9]). A boson mapping, which is an extension of the OAI mapping, has also been introduced in Ref. [9]. The IBM-2 parameters have been evaluated via this mapping. These parameters characterize some properties of the quadrupole collective states.

### III. ENERGIES OF MIXED-SYMMETRY STATES WITH $H^2$ CM

We shall discuss, in this section, the structures of the eigenstates obtained within the renormalized  $SD$  space via the  $H^2$ CM, for  $^{56}\text{Fe}$ ,  $^{54}\text{Cr}$ ,  $^{58}\text{Fe}$  and  $^{56}\text{Cr}$ . The excitation energies and the  $F$ -spin contents of lower-lying states are tabulated in Table I. The  $F$ -spin values for the renormalized  $SD$ -states are defined through the  $F$ -spin values of their IBM-2 images [9]. It is seen that the lowest  $0^+$  and  $2^+$  states are highly dominated by the symmetric

components. Though not all the states presented in Table I have one-to-one correspondence to the shell-model eigenstates, their identities seem to be maintained to a good extent, as will be discussed in Sect. IV.

### A. Mixed-symmetry $2^+$ state

In all the nuclei under investigation, the lowest state dominated by the mixed-symmetry (MS) component has  $J^P = 2^+$ ; it is the second  $2^+$  state in the  $SD$  space of  $^{56}\text{Fe}$  and  $^{54}\text{Cr}$ , while in  $^{58}\text{Fe}$  and  $^{56}\text{Cr}$  it is the third  $2^+$  state. This is a clear indication, derived from a microscopic and realistic standpoint, that the MS  $2^+$  state is lower than any other MS states in these nuclei. The excitation energy of these MS  $2^+$  states are 3.1–3.7 MeV, somewhat dependent on the nuclide.

Even though the  $F$ -spin is good for the  $0_1^+$  and  $2_1^+$  states, it is not trivial how pure the  $F$ -spin is in the MS-dominant states, because there may be some symmetric components around the lowest-lying MS components. As is shown in Table I, the  $F$ -spin purity of the second  $2^+$  state of  $^{56}\text{Fe}$  is excellent. This is consistent with the earlier analysis in Ref. [7]. Thus the  $F$ -spin plays a significant role in classifying the collective states of  $^{56}\text{Fe}$ .

In contrast to  $^{56}\text{Fe}$ , there is a certain amount of mixing between totally symmetric and MS components in the other three nuclei. Among them,  $^{56}\text{Cr}$  has a relatively good  $F$ -spin purity for the MS-dominated  $2^+$  state. This can be discussed in association with the IBM-2 hamiltonian, which has been derived via the extended OAI mapping in Ref. [9]. The  $F$ -spin purity correlates mainly with the  $\chi$  parameters of the bosonic  $\hat{Q}_\pi \cdot \hat{Q}_\nu$  interaction, since  $\epsilon_{d_\pi}$  and  $\epsilon_{d_\nu}$  have rather close values to each other. In  $^{56}\text{Fe}$  and  $^{56}\text{Cr}$ , the  $F$ -spin breaking due to the  $\hat{Q}_\pi \cdot \hat{Q}_\nu$  interaction is expected to be small, because  $\chi_\pi \approx \chi_\nu$  (see Table II of Ref. [9]). It is noticed from Table I that the influence of the  $F = F_{\text{max}} - 2$  component, which can be present in  $^{56}\text{Cr}$ , is quite small. Although the lack of the  $|D_\pi^2; 0^+\rangle$  component in the Cr nuclei prohibits the  $F$ -spin from being pure, this does not seriously influence the lower-lying states.

### B. Mixed-symmetry $1^+$ state

For the same reason as in the IBM-2, we have no symmetric  $1^+$  basis in the  $SD$  space of any nucleus. The lowest  $1^+$  state in the  $SD$  space should therefore have  $F = F_{\max} - 1$  (*i.e.*, MS state). The H<sup>2</sup>CM yields 3.7–4.8 MeV excitation energy for the lowest collective  $1^+$  state of these Cr-Fe nuclei ( $^{56}\text{Fe}$ ,  $^{54}\text{Cr}$ ,  $^{58}\text{Fe}$  and  $^{56}\text{Cr}$ ).

### C. Mixed-symmetry $3^+$ state

There is only a single  $3^+$  basis in the  $SD$  space of  $^{56}\text{Fe}$ , which is the MS one. For  $^{54}\text{Cr}$ ,  $^{58}\text{Fe}$  and  $^{56}\text{Cr}$ , we have symmetric  $3^+$  bases as well as MS  $3^+$  ones. The symmetric components contain three  $D$ -pairs at least, while one of the MS bases consists only of two  $D$ -pairs. It is of interest which component dominates the lowest collective  $3^+$  state. According to the present calculation, the lowest collective  $3^+$  state is dominated by the MS component in these nuclei, with the excitation energy of 3.9–4.2 MeV, as is presented in Table I. As well as the excitation energy, the admixture of the symmetric component is stable among the three nuclei (20–30%).

The MS  $1^+$  state is relatively easy to observe [1]. It is worth discussing the position of the MS  $3^+$  state relative to the MS  $1^+$  state.

In the IBM-2, the lowest MS  $1^+$  and  $3^+$  states are approximately expressed as

$$|1_M^+\rangle \propto [d_\pi^\dagger d_\nu^\dagger]^{(1)} |0_c^+(N_\pi^B - 1, N_\nu^B - 1)\rangle, \quad (2)$$

$$|3_M^+\rangle \propto [d_\pi^\dagger d_\nu^\dagger]^{(3)} |0_c^+(N_\pi^B - 1, N_\nu^B - 1)\rangle, \quad (3)$$

where the core state  $|0_c^+(N_\pi^B - 1, N_\nu^B - 1)\rangle$  is an appropriately chosen totally-symmetric  $0^+$  state with  $(N_\pi^B - 1)$  proton-bosons and  $(N_\nu^B - 1)$  neutron-bosons. If the nuclear shape does not strongly depend on the boson number,  $|0_c^+(N_\pi^B - 1, N_\nu^B - 1)\rangle$  can be taken as the ground state with the corresponding boson numbers. Neglecting the difference in coupling of the  $d_\pi d_\nu$  part to the  $|0_c^+(N_\pi^B - 1, N_\nu^B - 1)\rangle$  core, we reach an approximation for the relative energy as



$$\begin{aligned}
E(3_M^+) - E(1_M^+) &= \langle 3_M^+ | H^B | 3_M^+ \rangle - \langle 1_M^+ | H^B | 1_M^+ \rangle \\
&\approx \langle d_\pi d_\nu; 3^+ | H^B | d_\pi d_\nu; 3^+ \rangle - \langle d_\pi d_\nu; 1^+ | H^B | d_\pi d_\nu; 1^+ \rangle,
\end{aligned} \tag{4}$$

with the boson hamiltonian denoted by  $H^B$ . Note that this relation holds exactly in the group-theoretical limits  $U(5)_{\pi+\nu} \otimes SU_F(2)$ ,  $SU(3)_{\pi+\nu} \otimes SU_F(2)$  and  $O(6)_{\pi+\nu} \otimes SU_F(2)$  [12].

We here assume the following IBM-2 hamiltonian,

$$H^B = \sum_{\rho=\pi,\nu} \epsilon_{d_\rho} \hat{N}_{d_\rho} - \kappa \hat{Q}_\pi \cdot \hat{Q}_\nu + \sum_{J=1,2,3} \xi_J \hat{M}_J, \tag{5}$$

where

$$\hat{Q}_\rho = [d_\rho^\dagger s_\rho + s_\rho^\dagger \tilde{d}_\rho]^{(2)} + \chi_\rho [d_\rho^\dagger \tilde{d}_\rho]^{(2)}, \tag{6}$$

$$\hat{M}_J = [d_\pi^\dagger d_\nu^\dagger]^{(J)} \cdot [\tilde{d}_\nu \tilde{d}_\pi]^{(J)}, \quad \text{for } J = 1, 3, \tag{7}$$

$$\hat{M}_2 = \frac{1}{2} [d_\pi^\dagger s_\nu^\dagger - s_\pi^\dagger d_\nu^\dagger]^{(2)} \cdot [\tilde{d}_\pi s_\nu - s_\pi \tilde{d}_\nu]^{(2)}. \tag{8}$$

Though a more general IBM-2 hamiltonian has been derived in Ref. [9], this form is usually sufficient to discuss the basic structure of the low-lying states. Substituting the above hamiltonian (5) into Eq. (4), we obtain

$$E(3_M^+) - E(1_M^+) \approx \kappa \chi_\pi \chi_\nu + (\xi_3 - \xi_1). \tag{9}$$

The  $\kappa$  parameter is positive in physical cases, and is relatively insensitive to nuclide. If the  $(\xi_3 - \xi_1)$  term is negligible, the nucleus-dependence of  $E(3_M^+)$  relative to  $E(1_M^+)$  is essentially governed by the  $\chi_\pi \chi_\nu$  value.

The large positive  $\chi_\pi \chi_\nu$  value in  $^{56}\text{Fe}$ , which has been shown in Table II of Ref. [9], makes the MS  $3^+$  state substantially higher than the MS  $1^+$  state. The difference between  $\xi_1$  and  $\xi_3$  in this nucleus is not large enough to change this situation. On the other hand, we have  $\chi_\pi \chi_\nu \approx 0$  in  $^{54}\text{Cr}$ ,  $^{58}\text{Fe}$  and  $^{56}\text{Cr}$ . It should also be noticed that  $\xi_1 \approx \xi_3$  in these nuclei. Thereby comparable excitation energy is expected between the MS  $1^+$  and  $3^+$  states. Owing to admixture of the symmetric component, the MS-dominant  $3^+$  state appears even lower than the  $1^+$  state.

#### IV. DISTRIBUTIONS OF MIXED-SYMMETRY STATES

We have explicitly constructed the wavefunctions of the collective fermion states via the H<sup>2</sup>CM. This enables us to compare these states with the shell-model eigenstates, by calculating overlaps between their wavefunctions. In this section we shall investigate how the lower-lying collective states dominated by the MS components distribute over the shell-model eigenstates.

The overlaps of the MS  $2^+$  state of  $^{56}\text{Fe}$  with the shell-model eigenstates in  $E_x < 8$  MeV are shown in Fig. 1(a). A certain fragmentation of this  $2^+$  component occurs, because of the coupling to non-collective  $2^+$  states in its vicinity. It is found, however, that the main fraction is shared by the  $2_2^+$  and  $2_4^+$  states with more than 70% probability in total. This is consistent with the previous report in Ref. [7]. As is viewed in Table II, the summed probability of the MS  $2^+$  component in the shell-model eigenstates up to 5 MeV reaches as much as 80%. The fact that the collective-state amplitudes are concentrated in a relatively small energy range shows that we can regard the MS state as a basic building block. We can interpret this state as a doorway-type state.

Similarly, the doorway nature of the MS  $1^+$  state is clarified in the distribution over the shell-model eigenstates, as shown in Fig. 1(b). The  $1^+$  component is mainly shared by the shell-model  $1_2^+$  and  $1_3^+$  states, both of which exist around 3.5 MeV, with 87% probability in total.

The MS  $1^+$  component can be searched by using the  $M1$  transition to the ground state. Whereas the  $M1$  transition is forbidden for a purely spherical ground-state, even a small deformation makes it measurable. The following shell-model  $M1$  operator is adopted as in Refs. [7,9],

$$T(M1) = \sqrt{\frac{3}{4\pi}} \sum_{\rho=\pi,\nu} \left\{ g_{l,\rho}^{\text{eff}} \sum_{i \in \rho} l_i + g_{s,\rho}^{\text{eff}} \sum_{i \in \rho} s_i \right\}, \quad (10)$$

together with  $g_{l,\pi}^{\text{eff}} = g_{l,\pi}^{\text{free}} = 1.0[\mu_N]$ ,  $g_{l,\nu}^{\text{eff}} = g_{l,\nu}^{\text{free}} = 0.0[\mu_N]$ ,  $g_{s,\pi}^{\text{eff}} = 0.5g_{s,\pi}^{\text{free}}$  and  $g_{s,\nu}^{\text{eff}} = 0.5g_{s,\nu}^{\text{free}}$ . By employing this  $M1$  operator with the shell-model wavefunctions, the  $M1$  transition

strengths within the  $k \leq 2$  space are calculated and depicted in Fig. 3, with  $k$  denoting the number of nucleons excited out of  $0f_{7/2}$ . It should be recalled that the  $M1$  transition between totally symmetric states are forbidden within the IBM-2 framework [15]. On the other side, the  $M1$  transition between the ground state and the state with large MS component is expected to be measurable. Although the  $1^+$  states consisting of the  $k = 3$  configuration carry some  $M1$  strengths, their contribution will be important only in the higher energy region, as will be discussed further in Sect. V. The above spin-quenching factor has been fitted to the  $B(M1)$  values among lowest-lying states of  $^{56}\text{Fe}$  [7]. This factor is considerably smaller than the one predicted from microscopic standpoints [13], and may be ascribed to the influence of higher  $k$  configurations. It is noticed that a relatively strong influence of higher  $k$  configurations has been suggested for  $^{56}\text{Fe}$  on the basis of the electromagnetic properties [8]. It is found that the  $B(M1)$  distribution over low-lying states resembles the distribution of the MS component shown in Fig. 1(b). Both of the  $1_2^+$  and  $1_3^+$  states have relatively large  $B(M1)$  values to the ground state;  $0.04[\mu_N^2]$  from  $1_2^+$  and  $0.10[\mu_N^2]$  from  $1_3^+$ . The concentration of the MS  $1^+$  component around  $E_x \simeq 3.5$  MeV seems to be consistent with the recent  $(e, e')$  and  $(p, p')$  experiments reported in Ref. [14].

The distribution of the second  $2^+$  state in the collective space of  $^{54}\text{Cr}$  over the shell-model eigenstates is depicted in Fig. 2(a). The shell-model  $2_3^+$  state absorbs about  $\frac{2}{3}$  of the MS component, and more than 90% is exhausted by the states below 5 MeV, as shown in Table II. The MS-dominant  $2^+$  state also remains a basic mode through the doorway interpretation.

The lowest collective  $1^+$  and  $3^+$  components of  $^{54}\text{Cr}$  are confirmed to have similar nature, as presented in Fig. 2(b) and (c). The shell-model  $1_3^+$  and  $3_1^+$  states have large fractions of the MS states. Although both these states have not been observed, their MS-dominance is probably seen experimentally by the  $M1$  or  $M3$  excitation. As well as the  $M1$  transition, the  $M3$  transition may be sizable between the ground state and the MS state. According to the shell-model calculation, we predict  $B(M1; 1_3^+ \rightarrow 0_1^+) \simeq 0.23[\mu_N^2]$  and  $B(M3; 3_1^+ \rightarrow 0_1^+) \simeq 460[\mu_N^2\text{fm}^4]$ , by assuming the bare  $M3$  operator

$$T(M3) = \frac{\sqrt{21}}{2} \sum_{\rho=\pi,\nu} \left\{ g_{l,\rho}^{\text{free}} \sum_{i \in \rho} r_i^2 [Y^{(2)}(\hat{\mathbf{r}}_i) l_i]^{(3)} + 2g_{s,\rho}^{\text{free}} \sum_{i \in \rho} r_i^2 [Y^{(2)}(\hat{\mathbf{r}}_i) s_i]^{(3)} \right\}, \quad (11)$$

and the harmonic-oscillator single-particle wavefunctions with  $b = 1.956\text{fm}$ , as in Ref. [9]. The distribution of the low-lying  $M1$  and  $M3$  strengths is presented in Fig. 4, for the convenience of experimental search. The  $B(M3)$  value from  $3_1^+$  to the ground state is even larger than the Weisskopf unit, which is  $337[\mu_N^2\text{fm}^4]$  at  $A = 54$ . Moreover, the  $M3$  transition from  $3_1^+$  is notably stronger than those from neighboring  $3^+$  states, which may help us to identify the  $3_1^+$  state through a scattering experiment. We have a few strong  $M3$  strengths below 6 MeV, for states which have small fraction of the MS component. This is a notable contrast to the  $M1$  transition, which has a clear correlation to the distribution of the MS component. This happens mainly because the spin term in Eq. (11) has larger effects than in the  $M1$  case.

Figures 5 and 6 show the distributions of the collective states dominated by the MS components over the shell-model eigenstates, up to around 4 MeV, for the  $N = 32$  nuclei. Summed strengths are presented in Table II. Because of a numerical difficulty caused by the greater model space [9], the energy range in which the shell-model eigenstates are searched is restricted to a smaller region than in the  $N = 30$  nuclei. We mention a few points at this stage. There is a certain fragmentation for any of the collective MS-dominant states in the renormalized  $SD$  space. The fragmentation appears somewhat stronger in these  $N = 32$  nuclei than in the  $N = 30$  nuclei. Nevertheless, an appreciable portion of the collective component is already found in the low energy region, as is shown in Table II. We remark that the investigated energy range does not sufficiently exceed the energies of the lowest MS-dominant states in the renormalized  $SD$  space. This could be the reason why the probabilities of the MS component are so small for the  $N = 32$  nuclei, in comparison with the  $N = 30$  nuclei.

As stated in Sect. I, the fragmentation of the MS component over a small energy range has been observed for the scissors  $1^+$  states of heavier rotational nuclei. The situation looks quite similar to the current Cr-Fe case, suggesting the following global nature of lower-

lying MS states. It is inevitable for this type of collective components to fragment more or less, because there exist a certain number of non-collective degrees-of-freedom in the same energy region. While the coupling to the non-collective degrees-of-freedom leads to a certain fragmentation, the coupling is not so strong as for the MS states to lose their identity. The main fraction of the MS components remains in the vicinity of the original energy, and it is shared primarily by a few eigenstates. It is thus reasonable to regard the MS state as a doorway state.

## V. $B(M1)$ DISTRIBUTION IN $^{56}\text{Fe}$ AND $^{54}\text{Cr}$

The  $M1$  transition seems to be a good probe in investigating the MS  $1^+$  component. As has been shown in Sect. IV, the low-lying  $M1$  transition strengths correspond well to the MS  $1^+$  component. In this section, we research the  $B(M1)$  distribution covering a wider energy range, which will be useful for future experiments. We shall restrict ourselves to  $^{56}\text{Fe}$  and  $^{54}\text{Cr}$ , in order to avoid computational difficulties in  $^{58}\text{Fe}$  and  $^{56}\text{Cr}$ .

### A. Summed strengths and central energies

As in the Gamow-Teller (GT) transition [16], a certain part of the  $M1$  strengths is carried by the  $1^+$  states with the  $k = 3$  configuration, even if the ground state is described only by the  $k \leq 2$  configurations. Therefore, when we study the  $B(M1)$  distribution including a relatively high energy region with the  $k \leq 2$  ground-state wavefunction, we should not discard the  $k = 3$  configuration for the  $1^+$  states. For this reason, in the following we treat the  $1^+$  states in the  $k \leq 3$  space, keeping the ground state in the  $k \leq 2$  space. In fact, there should be a certain admixture of the  $k = 3$  configuration in the low-lying  $1^+$  states, although their influence will be small and may be taken into account by adjusting the single-particle parameters. Though the  $B(M1)$  values among low-lying states have been reproduced by the  $M1$  operator of Eq. (10) within the  $k \leq 2$  space, the single-particle parameters adopted there reflect the influence of the  $k = 3$  configuration to some extent. There is no reason to

apply the same parameters to the calculation involving the  $k = 3$  configuration explicitly. We here use, for convenience, the  $M1$  operator with the single-particle parameters evaluated by Towner [13] from microscopic viewpoints.

Table III exhibits, for  $^{56}\text{Fe}$  and  $^{54}\text{Cr}$ , the summed  $B(M1)$  values from all the possible  $1^+$  states to the ground state. The summed  $M1$  strength for each isospin component is shown, as well as the total strength. Note that, if the isospin of the ground state is denoted by  $T_0$  (*i.e.*,  $T_0 = 2$  for  $^{56}\text{Fe}$  and  $T_0 = 3$  for  $^{54}\text{Cr}$ ),  $T = T_0$  and  $T_0 + 1$  are possible for the  $1^+$  states. The summed  $B(M1)$  values are actually calculated as follows: we first generate the following state, which exhaust the non-energy-weighted sum,

$$|1_{\text{sum}}^+\rangle \equiv \mathcal{N} T(M1)|0_1^+\rangle, \quad (12)$$

where  $\mathcal{N}$  stands for a normalization constant. The total  $B(M1)$  value is equal to  $\mathcal{N}^{-2}$ . We next carry out the isospin projection for  $|1_{\text{sum}}^+\rangle$ , and the probability of each isospin component in  $|1_{\text{sum}}^+\rangle$  gives the ratio of the  $M1$  strengths between the isospin-conserving ( $T = T_0$ ) and isospin-raising ( $T = T_0 + 1$ ) components. If one wishes to obtain the  $M1$  excitation strengths from the ground state, the shown  $B(M1)$  values should be multiplied by a factor of three. It is noted that the isospin decomposition of the  $M1$  strength is important in some cases; for example, it yields significant information on the double- $\beta$ -decay matrix-element [17], via the close relation of  $M1$  to the GT transition.

Table III also shows the central energies of the  $M1$  strengths,

$$\bar{E}_x \equiv \frac{\sum_i E_x(1_i^+) B(M1; 1_i^+ \rightarrow 0_1^+)}{\sum_i B(M1; 1_i^+ \rightarrow 0_1^+)}. \quad (13)$$

At first glance, this appears to be obtained by  $\langle 1_{\text{sum}}^+ | P_T H P_T | 1_{\text{sum}}^+ \rangle / \langle 1_{\text{sum}}^+ | P_T | 1_{\text{sum}}^+ \rangle$ , where  $H$  indicates the shell-model hamiltonian in the  $k \leq 3$  space and  $P_T$  denotes the isospin projector. However, the following corrections are necessary. There is a certain difference in the ground-state energy between the  $k \leq 2$  and  $k \leq 3$  spaces. Although  $\bar{E}_x$  should be measured from the  $k \leq 3$  ground-state energy, it is not easy to compute the ground-state energy in the  $k \leq 3$  space because of its large dimensionality (about  $2 \times 10^6$  in the  $M$ -scheme). It is remarked that, as far as the energy intervals among low-lying  $1^+$  states are

concerned, the  $k \leq 3$  space has been confirmed to yield almost the same values as the  $k \leq 2$  space. To circumvent the time-consuming computation, we shift the  $T = T_0$   $1^+$  levels so that  $E_x(1_1^+)$  in the  $k \leq 3$  space becomes equal to that obtained in the  $k \leq 2$  space [8]. Regarding the  $T = T_0 + 1$  case, we adjust the  $T = T_0 + 1$  levels, by using the data of the neighboring nuclei [18]. For  $^{56}\text{Fe}$ , the energy of the lowest  $1^+$  state with  $T = 3$  is extracted from  $E_x(1_1^+)$  of  $^{56}\text{Mn}$  and the mass difference between  $^{56}\text{Fe}$  and  $^{56}\text{Mn}$ . For the Coulomb-energy difference, we apply the formula derived from the uniform charge-distribution,

$$\Delta E_C = \frac{e^2}{4\pi} \frac{3}{5r_C A^{1/3}} [Z^2 - (Z-1)^2] \simeq 0.696(2Z-1)A^{-1/3} \text{ MeV} \quad (r_C = 1.24\text{fm}). \quad (14)$$

The energy of the  $T = 4$   $1^+$  component of  $^{54}\text{Cr}$  is corrected in a similar manner, by using the  $^{54}\text{V}$  data. Although the  $1_1^+$  level has not been confirmed in  $^{54}\text{V}$  [18], we assume that the second excited state is  $1_1^+$  according to systematics of  $N = 31$  nuclei. The estimate of the Coulomb-energy difference might not be very precise. However, the presented  $\bar{E}_x$  values could be a guidance to future experiments.

## B. Mixed-symmetry component

The  $B(M1)$  distribution is calculated for each isospin component via Whitehead's moment method [19], starting from  $P_T|1_{\text{sum}}^+\rangle$  with 45 iterations. The results are given in Figs. 7 and 8, where the  $B(M1)$  values to the ground state are displayed by bins of 1 MeV. The spin-excitation strengths are calculated by setting  $g_{l,\rho} = 0$  ( $\rho = \pi, \nu$ ) in the  $M1$  operator, and are also displayed in Figs. 7 and 8.

For  $^{56}\text{Fe}$  presented in Fig. 7, the energies of the lowest three  $1^+$  levels are convergent in the iteration of Whitehead's moment method. As well as the energy intervals among these levels, the  $B(M1)$  values are close to those given in Sect. IV; and  $B(M1; 1_3^+ \rightarrow 0_1^+) = 0.11\mu_N^2$ . Thus, for the  $M1$  strengths from these low-lying states, the influence of the difference in size of the model space is absorbed into the single-particle parameters.

In Fig. 7, we see a low peak at 3–4 MeV for the  $T = T_0 = 2$  part, well below the main peak at around 8 MeV. The excitation regarding the orbital angular-momentum highly

dominates this peak. The  $1_2^+$  and  $1_3^+$  states form this low-energy peak. As it has been shown in Sect. IV, the  $1_2^+$  and  $1_3^+$  share the main fraction of the MS component. Notice that the MS component has  $T = T_0 = 2$ , and has been described by the  $k \leq 2$  configurations in Sect. IV, which should dominate the low-lying states. Therefore, the distribution of the MS  $1^+$  component shown in Sect. IV is connected to the low-energy part of the entire  $M1$  distribution.

For  $^{54}\text{Cr}$ , the energies of the low-lying  $1^+$  levels are not sufficiently convergent with 45 iterations. Still, the energy intervals among several lowest-lying components appear to be similar to those obtained in the  $k \leq 2$  space. We also notice a peak around 4 MeV separated from the main peak (see Fig. 8), thus indicating that the MS component is observable via the low-energy  $M1$  peak. This peak is predominantly constituted by the excitation of the orbital angular-momentum, as in  $^{56}\text{Fe}$ .

### C. Spin excitation

We next turn to the main peaks of the  $B(M1)$  distribution. The main peak for the  $T = T_0$  strengths (see Figs. 7 and 8) is dominated by the single-particle excitation from the  $j = l + 1/2$  orbit to its spin-orbit partner  $j' = l - 1/2$ . Such an excitation is often called spin excitation, because it is mainly contributed by the nucleon-spin operator, as shown below. The high-energy tail of the peak is low but damps very gradually. The  $B(M1)$  value up to 12 MeV amounts to 93% (94%) of the whole sum of  $T = T_0$  strengths, for  $^{56}\text{Fe}$  ( $^{54}\text{Cr}$ ). Therefore caution will be necessary in looking at experimental data on the summed  $B(M1)$  values: it is hard to extract the isospin-conserving  $M1$  strength by experiments with better precision than 10%.

For  $^{56}\text{Fe}$ , the  $M1$  distribution below 15 MeV has been investigated experimentally [1]. The pattern of the distribution is reproduced well by the present calculation.

It is found in Fig. 7 that, around the main peak, the  $M1$  strengths due only to the spin terms are substantially greater than the  $B(M1)$  values containing all contributions.



Namely, although the spin contribution is dominant in this peak, there exists a certain destructive contribution of the orbital angular-momentum. This is explained in a simple way as follows. Let us consider the single-particle matrix-element  $\langle j' = l - 1/2 || T(M1) || j = l + 1/2 \rangle$ . Since  $\langle j' = l - 1/2 || j || j = l + 1/2 \rangle = 0$ , we have  $\langle j' = l - 1/2 || l || j = l + 1/2 \rangle = -\langle j' = l - 1/2 || s || j = l + 1/2 \rangle$ . Neglecting the  $[Y^{(2)}s]$ -term in the  $M1$  operator, we obtain  $\langle j' = l - 1/2 || T(M1) || j = l + 1/2 \rangle \propto (g_s - g_l)$  [20]. Because  $|g_s|$  is appreciably larger than  $|g_l|$ , the spin contribution is dominant in this excitation, as has been stated above. On the other hand, the orbital contribution should be present, as far as the  $M1$  transition involves proton excitations. Therefore, except for the proton  $LS$ -closed nuclei, the spin excitation should contain a destructive contribution from the orbital angular-momentum. We thus need caution in extracting the  $B(M1)$  values from  $(p, p')$  experiments, which hardly excite the orbital motion owing to the locality of the  $NN$  interaction:  $(p, p')$  tends to overestimate the  $B(M1)$  values around the peak region. For  $^{54}\text{Cr}$  (see Fig. 8), the destructive orbital contribution to the spin excitation is confirmed by summing the  $M1$  strengths in the 7–10 MeV region, though it is not apparent for individual bins because of the poor convergence.

The main fraction of the  $T = T_0 + 1$  strengths, which are also shown in Fig. 7 for  $^{56}\text{Fe}$  and Fig. 8 for  $^{54}\text{Cr}$ , seems to be distinct in energy from the main body of the  $T = T_0$  strengths, besides the reliability of the estimated excitation energy. The peak appears to be high enough as not to be hidden in the  $T = T_0$  component. However, the tail of the  $T = T_0$  component amounts to about 10% for each bin relative to the  $T = T_0 + 1$  peak height. Even if the peak can be observed clearly, it will not be easy to obtain the isospin-raising strength from  $M1$  excitation experiments with a high precision. While the spin degrees-of-freedom give the main contribution to the  $T = T_0 + 1$   $M1$  strengths, the orbital angular-momentum contributes destructively, by the same mechanism as in the  $T = T_0$  case.

## VI. SUMMARY AND DISCUSSION

By applying the  $H^n$ -cooling method ( $H^n$ CM) with  $n = 2$ , the IBM-2 picture is extracted from the large-scale shell-model results for  $^{56}\text{Fe}$ ,  $^{54}\text{Cr}$ ,  $^{58}\text{Fe}$  and  $^{56}\text{Cr}$ . The lower-lying MS states are investigated with a particular interest: the distributions of these components are seen in terms of the overlaps between the wavefunctions in the renormalized  $SD$  space and the shell-model eigenfunctions. In  $^{56}\text{Fe}$  and  $^{54}\text{Cr}$ , the MS states are shown to be basic modes, while weak fragmentation is inevitable because of the high level density. Therefore, the doorway interpretation is appropriate for the MS states. This consequence is consistent with the behavior of the scissors  $1^+$  state observed in heavier nuclei. Despite the smaller energy range of investigation, there is no contradiction either in  $^{58}\text{Fe}$  nor  $^{56}\text{Cr}$  with the doorway nature of the lower-lying MS states.

In addition to Ref. [7], Halse studied quadrupole collective modes including the MS ones in the Cr-Fe nuclei [21]. His work has been based on a more severely truncated shell-model calculation assuming the  $^{56}\text{Ni}$  inert core [22], which does not reproduce the energy levels beyond 3 MeV precisely. The predicted energies of the MS-dominant states are not so different from the present one, though the fragmentation of those components was out of scope in that work.

We show a clear evidence that the lowest MS-dominant state has  $J^P = 2^+$  for these nuclei. There have been several theoretical and experimental suggestions, in this mass region [6,21] as well as in heavier-mass region [23], that the lowest MS state has  $J^P = 2^+$  for some nuclei. This expectation is confirmed by the present realistic study. The indication of the MS  $3^+$  state is also obtained. It is almost the first realistic calculation on the MS  $3^+$  state, except the study based on the  $M3$  transition in lighter  $pf$ -shell region [24].

The low-lying  $M1$  strengths to the ground state are calculated for  $^{56}\text{Fe}$  and  $^{54}\text{Cr}$ . The  $M1$ -strength distribution resembles the distribution of the MS  $1^+$  component. It is hopeful to search the MS  $1^+$  component experimentally. The  $M3$  strength is also calculated for  $^{54}\text{Cr}$ . Despite a certain additional contribution of non-collective degrees-of-freedom, the MS

$3^+$  component may be detectable by scattering experiments. The  $B(M1)$  distribution in a wider energy range, as well as the summed  $B(M1)$  values, are also presented, for the isospin-conserving and isospin-raising components, respectively. Unlike the RPA approach, we can treat the isospin correctly. The MS  $1^+$  component forms a peak in the low-energy region, and is well separated from the main peak of the spin excitation. Concerning the summed  $M1$  strength, it is found that the tail of the  $B(M1)$  distribution may contribute by about 10%. The isospin-raising component seems to have a distinct peak from the isospin-conserving one. The destructive contribution of the orbital angular-momentum is confirmed both for the isospin-conserving and isospin-raising spin excitations.

### ACKNOWLEDGMENTS

The authors are grateful to Prof. A. Gelberg for careful reading the manuscript.

## REFERENCES

- [1] A. Richter, in *Perspectives for the Interacting Boson Model: on the Occasion of Its 20th Anniversary*, edited by R. F. Casten, A. Vitturi, A. B. Balantekin, B. R. Barrett, J. N. Ginocchio, G. Maino and T. Otsuka (World Scientific, Singapore, 1994), p.59.
- [2] F. Iachello, Nucl. Phys. **A358**, 89c (1981);  
A. E. L. Dieperink, Prog. Part. Nucl. Phys. **9**, 121 (1983).
- [3] T. Suzuki and D. J. Rowe, Nucl. Phys. **A289**, 461 (1977);  
N. Lo Iudice and F. Palumbo, Phys. Rev. Lett. **41**, 1532 (1978); Nucl. Phys. **A326**, 193 (1979);  
R. R. Hilton, Z. Phys. **A316**, 121 (1984);  
E. Lipparini and S. Stringari, Phys. Lett. **B130**, 139 (1983).
- [4] F. Iachello, Phys. Rev. Lett. **53**, 1427 (1984);  
T. Otsuka and J. N. Ginocchio, Phys. Rev. Lett. **54**, 777 (1985).
- [5] R. Nojarov and A. Faessler, J. Phys. **G13**, 337 (1987);  
K. Heyde and J. Sau, Phys. Rev. C **33**, 1050 (1986).
- [6] S. A. A. Eid, W. D. Hamilton and J. P. Elliott, Phys. Lett. **B166**, 267 (1986);  
S. P. Collins *et al.*, J. Phys. **G15**, 321 (1989);  
K. P. Lieb *et al.*, Phys. Lett. **B215**, 50 (1988);  
J. Takamatsu *et al.*, Colloque de Physique **C6**, 423 (1990).
- [7] H. Nakada, T. Otsuka and T. Sebe, Phys. Rev. Lett. **67**, 1086 (1991).
- [8] H. Nakada, T. Sebe and T. Otsuka, Nucl. Phys. **A571**, 467 (1994).
- [9] H. Nakada and T. Otsuka, Phys. Rev. C, in press.
- [10] T. T. S. Kuo and G. E. Brown, Nucl. Phys. **A114**, 241 (1968).
- [11] T. Otsuka, A. Arima and F. Iachello, Nucl. Phys. **A309**, 1 (1978).

- [12] F. Iachello and A. Arima, *The Interacting Boson Model* (Cambridge University Press, Cambridge, 1987).
- [13] I. S. Towner, Phys. Rep. **155**, 263 (1987).
- [14] A. Richter, in *Proceedings of 4th International Spring Seminar on Nuclear Physics: The Building Blocks of Nuclear Structure*, edited by A. Covello (World Scientific, Singapore, 1993), p.335.
- [15] O. Scholten *et al.*, Nucl. Phys. **A438**, 41 (1985).
- [16] H. Nakada and T. Sebe, J. Phys. **G22**, 1349 (1996).
- [17] H. Nakada, T. Sebe and K. Muto, Nucl. Phys. **A607**, 235 (1996).
- [18] R. B. Firestone and V. S. Shirley, *Table of Isotopes, 8th edition* (John Wiley & Sons, New York, 1996).
- [19] R. R. Whitehead, in *Moment Methods in Many Fermion Systems*, edited by B. J. Dalton, S. M. Grimes, J. D. Vary and S. A. Williams (Plenum, New York, 1980), p.235.
- [20] A. Bohr and B. R. Mottelson, *Nuclear Structure*, vol. 1 (Benjamin, New York, 1969), p.337.
- [21] P. Halse, Phys. Rev. C **41**, 2340 (1990); Phys. Rev. C **44**, 2467 (1991).
- [22] H. Horie and T. Ogawa, Prog. Theor. Phys. **46**, 439 (1971); Nucl. Phys. **A216**, 407 (1973).
- [23] W. D. Hamilton, A. Irbäck and J. P. Elliott, Phys. Rev. Lett. **53**, 2469 (1984).
- [24] L. Zamick, Phys. Rev. C **33**, 691 (1986);  
H. Liu and L. Zamick, Phys. Rev. C **36**, 2064 (1987).

# TABLES

TABLE I.  $F$ -spin probabilities (%) of the states in the renormalized  $SD$  space via the  $H^2CM$ .

Nucleus	$J^P$	$E_x(\text{MeV})$	$F = F_{\text{max}}$	$F = F_{\text{max}} - 1$
$^{56}\text{Fe}$	$0^+$	0.000	100.0	0.0
	$1^+$	3.746	0.0	100.0
	$2^+$	1.088	99.9	0.1
	$2^+$	3.568	0.1	99.9
	$3^+$	4.835	0.0	100.0
$^{54}\text{Cr}$	$0^+$	0.000	91.0	9.0
	$1^+$	4.378	0.0	100.0
	$2^+$	1.034	92.1	7.9
	$2^+$	3.171	44.7	55.3
	$3^+$	4.148	20.1	79.9
$^{58}\text{Fe}$	$0^+$	0.000	95.2	4.8
	$1^+$	4.707	0.0	100.0
	$2^+$	1.171	91.4	8.6
	$2^+$	2.689	69.0	31.0
	$2^+$	3.697	37.7	62.3
	$3^+$	3.922	25.2	74.8
$^{56}\text{Cr}$	$0^+$	0.000	93.2	3.4
	$1^+$	4.786	0.0	100.0
	$2^+$	1.301	92.6	4.7
	$2^+$	2.730	81.8	15.3
	$2^+$	3.462	13.8	83.6
	$3^+$	4.108	26.4	72.3

TABLE II. Summed probabilities of the MS-dominant components over the shell-model eigenstates. The energy range for the summation is also shown.

Nucleus	$J^P$	Energy range	Prob. (%)
$^{56}\text{Fe}$	$1^+$	$E_x < 5 \text{ MeV}$	87
	$2^+$	$E_x < 5 \text{ MeV}$	79
$^{54}\text{Cr}$	$1^+$	$E_x < 5 \text{ MeV}$	83
	$2^+$	$E_x < 5 \text{ MeV}$	94
	$3^+$	$E_x < 5 \text{ MeV}$	88
$^{58}\text{Fe}$	$1^+$	$E_x < 4.5 \text{ MeV}$	63
	$2^+$	$E_x < 3.8 \text{ MeV}$	68
	$3^+$	$E_x < 4 \text{ MeV}$	41
$^{56}\text{Cr}$	$1^+$	$E_x < 4.5 \text{ MeV}$	46
	$2^+$	$E_x < 3.9 \text{ MeV}$	78
	$3^+$	$E_x < 4.1 \text{ MeV}$	57

TABLE III. Summed  $B(M1)$  values and their central energies.

Nucleus		$\sum B(M1) (\mu_N^2)$	$\bar{E}_x \text{ (MeV)}$
$^{56}\text{Fe}$	$T = 2$	4.22	9.1
	$T = 3$	0.88	18.2
	total	5.10	10.7
$^{54}\text{Cr}$	$T = 3$	4.20	8.6
	$T = 4$	0.24	29.0
	total	4.44	9.7

## FIGURE CAPTIONS

Fig.1: Distribution of the MS-dominant components over the shell-model eigenstates in  $^{56}\text{Fe}$ :

(a) the second  $2^+$  state and (b) the  $1^+$  state, obtained in the renormalized  $SD$  space via the  $H^2\text{CM}$ . The vertical axis shows squares of the overlaps.

Fig.2: Distribution of the MS-dominant components over the shell-model eigenstates in  $^{54}\text{Cr}$ :

(a) the second  $2^+$  state, (b) the first  $1^+$  state and (c) the first  $3^+$  state, obtained in the renormalized  $SD$  space.

Fig.3:  $B(M1)$  distribution from  $1^+$  states to the ground state in  $^{56}\text{Fe}$ , within the  $k \leq 2$  space.

Fig.4: (a)  $B(M1)$  and (b)  $B(M3)$  distribution to the ground state in  $^{54}\text{Cr}$ , within the  $k \leq 2$  space.

Fig.5: Distribution of the MS-dominant components over the shell-model eigenstates in  $^{58}\text{Fe}$ :

(a) the third  $2^+$  state, (b) the first  $1^+$  state and (c) the first  $3^+$  state, obtained in the renormalized  $SD$  space.

Fig.6: Distribution of the MS-dominant components over the shell-model eigenstates in  $^{56}\text{Cr}$ :

(a) the third  $2^+$  state, (b) the first  $1^+$  state and (c) the first  $3^+$  state, obtained in the renormalized  $SD$  space.

Fig.7:  $B(M1)$  distribution to the ground state in  $^{56}\text{Fe}$ , for  $1^+$  states with  $T = 2$  and  $T = 3$ .

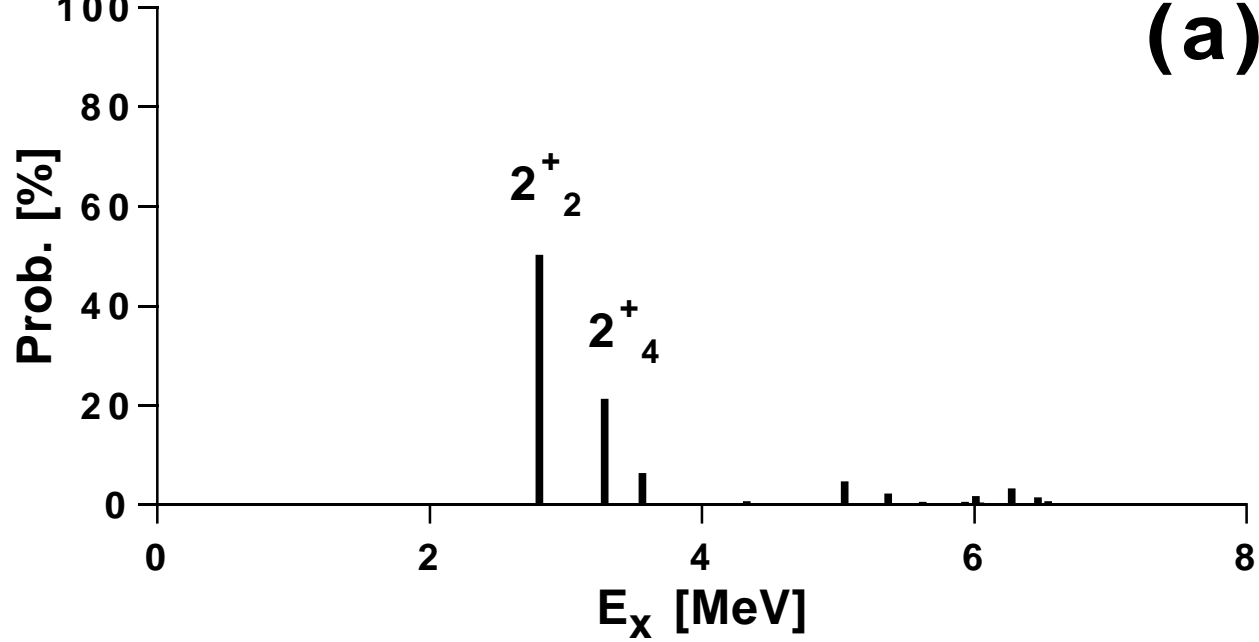
The values without orbital contribution are indicated by the short bars.

Fig.8:  $B(M1)$  distribution to the ground state in  $^{54}\text{Cr}$ , for  $1^+$  states with  $T = 3$  and  $T = 4$ .

The values without orbital contribution are indicated by the short bars.



**(a)**



**(b)**

